Korean J. Chem. Eng., 35(2), 428-437 (2018)
DOI: 10.1007/s11814-017-0308-6

pISSN: 0256-1115
eISSN: 1975-7220

Co-pyrolytic behaviors of biomass and polystyrene: Kinetics, thermodynamics and evolved gas analysis

Gamzenur Özsin† and Ayşe Eren Pütün

Department of Chemical Engineering, Faculty of Engineering, Anadolu University, Eskişehir, 26555, Turkey
(*Received 2 July 2017 • accepted 5 November 2017*)

Abstract−The pyrolytic degradation mechanism of chestnut shell (CNS) and its blend with waste polystyrene (PS) were investigated. Individual pyrolysis behavior of samples obtained separately was compared with those of the blends using a combined TGA/MS/FT-IR system. To elaborate kinetic analysis and to determine kinetic parameters, distributed activation energy model (DAEM) was used. The average activation energy of co-pyrolytic decomposition reaction was 191.6 kJ/mol, while the activation energy of the pyrolysis of CNS and PS was 175.2 and 208.9 kJ/mol, respectively. Friedman and Flynn-Wall-Ozawa iso-conversional methods were applied and the results were found to be consistent with the models. To express the presence of complex reaction mechanisms and the interactions of the radicals, thermodynamic parameters were also calculated. Finally, the pathways for main volatiles were established, and their relationship with the pyrolytic degradation was suggested.

Keywords: Biomass, Polystyrene, Pyrolysis, TGA/MS/FT-IR, Kinetic, Thermodynamic

INTRODUCTION

Plastics are one of the most engineered materials due to their great versatility, low weight and excellent electrical and thermal insulation properties. As a result of these superior properties, a drastic growth in polymer production has led to large amounts of plastic wastes that cause huge economic and environmental problems. On average, 25 million tons of post-consumer plastic waste is generated in Europe per year. In 2014, 29.7% of this was effectively recycled, 39.5% was sent to energy recovery and the remaining amount of 30.8% was landfilled [1,2]. In recent years, more stringent legislations have forced waste disposal plants to convert the waste to energy. For instance, the European Commission pointed out energy recovery from wastes according to its future energy strategies [3]. Such an energy recovery from waste not only involves resource conservation, but also has positive effects from the climate protection point of view as well. There are several thermochemical conversion processes have drawn attention to obtain energy and material from wastes. Compared to the other thermochemical conversion methods, pyrolysis has the further advantages of yielding both liquid, solid and gaseous products. While petro-based chemicals or fuels can be obtained from pyrolysis liquid product, carbon black or activated carbon can be produced from the solid residues [4-15].

When it comes to creating clean and sustainable energy and materials via pyrolysis process, biomass usage seems advantageous because of environmental benefits, renewability, and accessibility all over the world [16]. It is known that co-processing of biomass with a variety of materials such as waste polymers creates considerable synergistic effects during pyrolytic degradation such as increasing product yields, enhancing product qualities and decreasing emission amounts [17-19]. An extensive bibliography is available regarding the pyrolytic behaviors of polymers such as low-density polyethylene (LDPE), high-density polyethylene (HDPE), polystyrene (PS), polyethylene terephthalate (PET), polyvinyl chloride (PVC), and their blends which evaluate radical interactions resulting from their H-donor effect [20-27]. Blending polymers to lignocellulosic biomass can lead to an increase in volatiles (such as carbon dioxide, carbon monoxide, hydrogen, and water) [28]. As a result, gas contact between primary volatiles and secondary cracking reactions can be enhanced. However, when biomass is degraded alone or together with polymers the decomposition mechanism differs due to chemical composition, the degree of crystallinity of components such as cellulose, hemicellulose, lignin and inorganics [29,30]. Therefore, it is impossible to reach a general statement on the effect of biomass during the co-pyrolysis.

In this study, a specific biomass sample, chestnut shell (CNS), and a polymer waste, PS, interactions during co-pyrolysis are investigated by thermogravimetric analysis/Fourier transform infrared spectroscopy/mass spectroscopy (TGA/FT-IR/MS) technique. TGA is one of the commonly used techniques to study thermal events during pyrolysis because of its experimental simplicity and reliability [31,32]. By coupling spectroscopic techniques such as FT-IR and MS to TGA, the measurement of primary gas evolved from thermochemical reactions together with the calculation of kinetic parameters is probable. By this way, optimal thermal processing temperatures, heating rates, and residence times for targeted volatilization of specific compounds can be determined, which is beneficial for controlling the process and assessing the feasibility and design of pyrolysis reactors [33,34]. PS and CNS are selected as raw materials since they comprise a significant amount of the plastic content of municipal solid waste of Turkey. Furthermore, CNS

†To whom correspondence should be addressed.
E-mail: gozsin@anadolu.edu.tr

has paid special attention among the numerous non-edible biomass wastes due to its abundance in the region. According to the statistics of the Food and Agriculture Organization of United Nations in 2015, Turkey is the third country in the world in terms of chestnut production with an approximate annual production of 60000 MT [35]. Therefore, large amounts of shells are discarded as a by-product of nut processing factories. Almost no study on the pyrolysis and co-pyrolysis of chestnut shell has been published yet to the best of our knowledge. In the scope of this study, the distributed activation energy model (DAEM) was employed to investigate the activation energy values during pyrolysis, and the results were compared with different iso-conversional techniques. Then, thermodynamic analyses together with evolved gas analysis were performed by simultaneous TGA/FT-IR and TGA/MS measurements.

MATERIALS AND METHODS

1. Experimental Study

1-1. Preparation and Characterization of Raw Materials

Chestnut shells were obtained from a chestnut candy factory, dried at room temperature and then ground to obtain a uniform particle size. Similar to the biomass sample, PS samples were obtained from waste plastic recycling plant and then ground and sieved. The same particle sizes were used in the experiments. Blends were prepared by mixing samples at a definite ratio of 50 wt%. A particle size range between 112 μm and 224 μm was used throughout the thermoanalytical measurements.

Prior to the TGA/FT-IR/MS experiments, proximate, ultimate and component analyses were performed. Ash (1.20 wt%) and moisture (10.17 wt%) content was relatively low and large amounts of volatile matter (65.55 wt%) were present in the structure of CNS. Fixed carbon content was calculated from the difference as 23.08 wt%. From the component consideration, higher lignin content (42.69 wt%) is noticeable for the biomass sample. Hemicellulose, cellulose, and extractive amounts were found as 22.64, 31.61 and 1.86 wt%, respectively. Ash analysis of chestnut shell was also performed by the XRF technique and results showed that CaO (43.7 wt%), K_2O (20.7 wt%) and SO_3 (7.2 wt%) contribute more to the inorganic phase than other constituents. Other than these organic phases, some typical inorganics, which can be found in biomass structure such as Na_2O, SiO_2, MnO, Fe_2O_3, were detected.

When ultimate analyses of CNS and PS were performed with an elemental analyzer (Leco 628 Series CHN-S) and elemental carbon content was found as 48.0 and 90.3 wt% while hydrogen content was as 5.5 and 9.1, respectively. Both samples include a minor amount of nitrogen, but oxygen content of biomass was significantly higher in CNS (45.9 wt%), considering the trace amounts (smaller than 0.1 wt%) in PS. As a result, H/C ratios of CNS and PS were obtained as 1.352 and 1.195, respectively. When the calorific value was evaluated, a higher heating value of PS (43.6 MJ/kg) was found higher than CNS (15.9 MJ/kg) due to higher elemental carbon content of PS.

1-2. Thermoanalytical Measurements

The thermoanalytical measurements were carried out under an inert atmosphere using a TGA device (Setaram-Labsys Evo) coupled to an FT-IR spectrometer (Thermo Scientific iz10) and a mass spectrometer (Pfeiffer Omni Star). A schematic representation of the experiment system is shown in Fig. 1. Approximately 10 mg of sample was loaded into the Al_2O_3 crucible to prevent the possible temperature gradient in the sample and ensure the kinetic control of the process. A mixing ratio of 1 : 1 (wt PS/wt biomass) was used for the co-pyrolysis experiments. Kinetic experiments were performed using linear heating rates from 5 to 40 °C/min, and results were monitored from 25 °C to 1,000 °C. All experiments were performed in triplicates.

Evolved gaseous species from the TGA furnace were detected by connecting MS and FT-IR to TGA. During measurements, transfer lines and gas cells were heated to avoid condensation and secondary reactions. Online FT-IR analysis was performed in the range of 4,000-400 cm^{-1}. MS was operated under a vacuum and detected the characteristic fragment ion intensity of the volatiles according

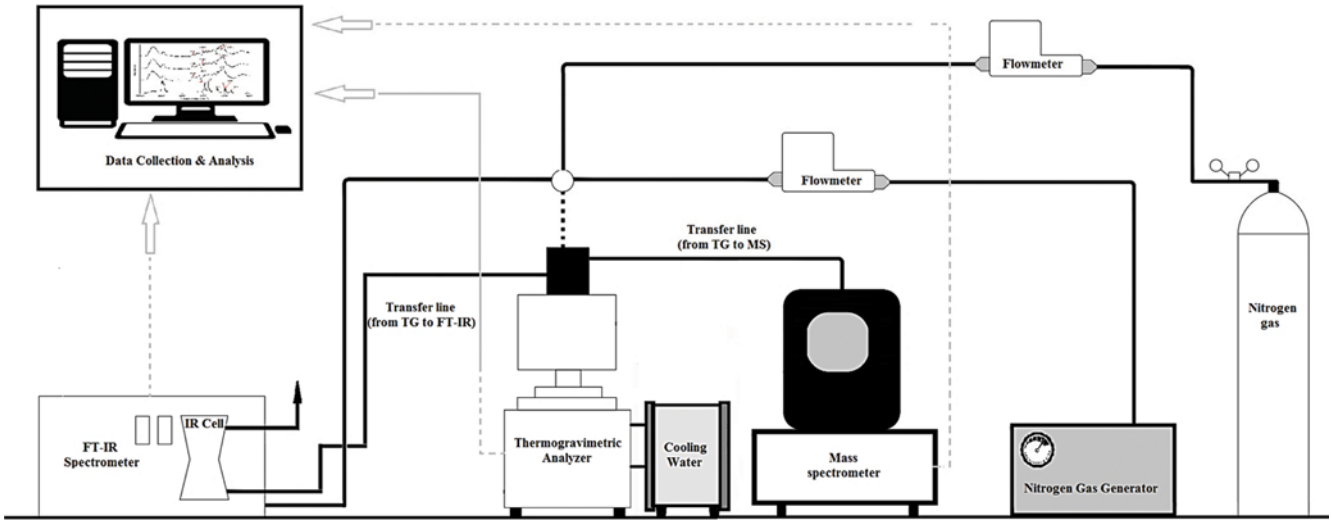

Fig. 1. Schematic representation of TG/FT-IR/MS system.

to their respective mass to charge ratios (m/z). A secondary electron multiplier (SEM) type detector was used during simultaneous measurements and intensities of gaseous products were first analyzed by evolution curves obtained by a preliminary scan. Then the signals of the selected compounds were recorded.

2. Kinetic Modelling

Pyrolytic degradation mechanism to interpret activation energy can be obtained from the experimental data collected by TGA. To have an insight into degradation behavior during co-pyrolysis, theoretical mass loss curves as a function of temperature were calculated as the sum of each individual material's weighted conversion and the formula is given as:

$$w_{theoretical}(T) = X_{CNS} w_{CNS} + X_{PS} w_{PS} \quad (1)$$

where X_{CNS} and X_{PS} are the weight fractions in the blend (which is 0.5 in the current study) and w_{CNS} and w_{PS} are the instantaneous weights of the components. Pyrolysis reactivity index (R_p) is calculated according to the following formula:

$$R_p = \frac{1}{w_o}\left(\frac{dw}{dt}\right)_{max} \quad (2)$$

where $(dw/dt)_{max}$ is the maximum pyrolysis rate and wo is the initial weight before the pyrolysis stage. Char yield (CY), at the end of the main pyrolysis zone was calculated by the following relationship:

$$CY(\%) = \frac{w_f}{w_0} x100 \quad (3)$$

where; w_0 and w_f are the initial sample mass and the mass at the end of the pyrolysis, respectively. On the other hand, fractional conversion is written by:

$$\alpha = \frac{w_o - w_t}{w_o - w_f} \quad (4)$$

where; w_t is the instantaneous sample mass at time t or temperature T. The basic rate equation of solid-state thermal conversion processes assumes that the conversion rate is proportional to the concentration of reactant and dependent on temperature. At a linear temperature heating rate (β); two different independent functions, namely temperature function (k(T)) and fractional conversion function (f(α)), are often used to define kinetic expression as given in Eq. (5):

$$\frac{d\alpha}{dt} = \beta\frac{d\alpha}{dT} = k(T) f(\alpha) \quad (5)$$

The temperature dependency of the rate constant, k, is described by Arrhenius equation [k=Aexp(−E_a/RT)]. Here, E_a is the activation energy, A the pre-exponential factor and R the gas constant. Hence, the reaction rate can be given in the form:

$$\beta\frac{d\alpha}{dT} = A\exp\left(-\frac{E_a}{RT}\right) f(\alpha) \quad (6)$$

where f(α) is the conversion function. Eq. (6) can also be integrated into;

$$\int_0^{\alpha}\frac{d\alpha}{f(\alpha)} = g(\alpha) = \frac{A}{\beta}\int_{To}^{T}\exp\left(-\frac{E_a}{RT}\right)dT \equiv \frac{AE_a}{\beta R} p(u) \quad (7)$$

where g(α) and p(u) are known as the integrated form of fractional conversion function, and temperature integral, respectively. Based on the kinetic methods applied, p(u) can be given by some mathematical approximations [36].

2-1. DAEM Approach

The DAEM assumes that a number of parallel, irreversible and first-order reactions with different energies occur simultaneously, reflecting variations in the bond strengths of species. According to the model developed by Miura [37], all frequency factors differ only in activation energy, and the number of independent reactions is large enough to permit continuous Gaussian distribution of the activation energy. Activation energy distribution defined in the DAEM approach is to be expressed as a function of f(E_a):

$$\int_0^{\infty} f(E_a)dE_a = 1 \quad (8)$$

Therefore, total amount of volatiles evolved up to time t is expressed in terms of f(E) by:

$$1-\alpha = \int_0^{\infty}\exp\left(-k_0\int_0^{t}\exp\left(\frac{E_a}{RT}\right)dt\right) f(E_a)dE_a \quad (9)$$

Sometimes the term V/V* is used to describe the reacted fraction (or conversion degree) instead of α (α=V*/V). In this form, V* and V refer to instantaneous and initial amount of volatile matter, respectively. The exponential function given in Eq. (9) is the so-called φ function. For a constant heating rate, φ function can be transformed from an integral in time to an integral in temperature as follows:

$$\varphi(E_a, T) = \exp\left(-k_0\int_0^{t}\exp\left(\frac{E_a}{RT}\right)dt\right) \cong \exp\left(-\frac{k_0}{\beta}\int_0^{T}\exp\left(\frac{E_a}{RT}\right)dT\right) \quad (10)$$

This function can be approximated by a step function at a value of E=E_a. Hence, Eq. (10) can be simplified as:

$$\alpha = \frac{V^*}{V} = 1 - \int_{E_a}^{\infty} f(E_a)dE_a = \int_0^{E_a} f(E_a)dE_a \quad (11)$$

Also, φ function can be approximated as:

$$\varphi(E, T) \cong \exp\left(-\frac{k_0 RT^2}{\beta E} e^{(-E_a/RT)}\right) \quad (12)$$

Choosing activation energy value to satisfy the condition of φ (E_a, T)=0.58 is convenient for the different k_o and f(E) combinations. Hence, the relationship between E_a, β, T and k_o can be expressed as:

$$-\ln(0.58)\frac{\beta E_a}{k_0 RT^2} = e^{(-E_a/RT)} \quad (13)$$

According to the DAEM approach, the reactions with an associated activation energy occur at a specific temperature and heating rate, which can be formulated as:

$$\frac{dV}{dt} \cong \frac{d(\Delta V)}{dt} = k_0 e^{(-E_a/RT)}(\Delta V^* - \Delta V) \quad (14)$$

For a constant value of k_o, corresponding to a determined reaction, integration of Eq. (14) gives Eq. (15) in the case of constant heating rate:

$$1-\frac{\Delta V}{\Delta V^{*}}=\exp\left(-k_0\int_0^t e^{(-E_a/RT)}dt\right)\cong\exp\left(-\frac{k_0RT^2}{\beta E_a}e^{(-E_a/RT)}\right) \quad (15)$$

By taking the double logarithm Eq. (15), Eq. (16) may be obtained as:

$$\ln\left(\frac{\beta}{T^2}\right)=\ln\left(\frac{k_0R}{E_a}\right)-\ln\left[-\ln\left(1-\frac{\Delta V}{\Delta V^{*}}\right)\right]-\frac{E_a}{RT} \quad (16)$$

Considering that $1-(\Delta V/\Delta V^{*})=\varphi(E_a, T)=0.58$, Eq. (16) can be simplified as:

$$\ln\left(\frac{\beta}{T^2}\right)=\ln\left(\frac{k_0R}{E_a}\right)+0.6075-\frac{E_a}{RT} \quad (17)$$

Eq. (17) is the so-called Arrhenius equation of DAEM that correlates the main kinetic parameters with the heating rate for a determined temperature.

2-2. Iso-conversional Methods

Iso-conversional methods enable the prediction of activation energies on conversion degree in a model-independent way that uses multiple temperature programs in order to gain data on different heating rates at a constant extent of conversion. To compare the activation energy values calculated by DAEM and check the consistency of the models, two commonly used iso-conversional methods, Friedman [38] and FWO [39,40], were also applied to the same data whose linearized final forms are given in Eq. (18) and Eq. (19), respectively.

$$\ln\left(\beta\frac{d\alpha}{dT}\right)=\ln A+\ln f(\alpha)-\frac{E_a}{RT} \quad (18)$$

$$\ln\beta=\ln\frac{AE_a}{Rg(\alpha)}-5.331-1.052\frac{E_a}{RT} \quad (19)$$

3. Thermodynamic Analysis

In analogy with kinetic analysis, pre-exponential factor, changes in enthalpy (ΔH), Gibbs free energy (ΔG) and entropy (ΔS) can be calculated using thermogravimetric analysis and expressed by Eqs. (20)-(23)

$$A=\left[\beta E_a\exp\left(\frac{E_a}{RT_m}\right)\right]/(RT_m^2) \quad (20)$$

$$\Delta H=E_a-RT \quad (21)$$

$$\Delta G=E_a+RT_m\ln\left(\frac{K_BT_m}{hA}\right) \quad (22)$$

$$\Delta S=\frac{\Delta H-\Delta G}{T_m} \quad (23)$$

where, A is pre-exponential factor (s^{-1}), T_m is peak temperature (K), K_B is Boltzmann constant (1.381×10^{-23} J/K) and h is the Planck constant (6.626×10^{-34} Js).

RESULTS

1. Thermal Analysis of CNS and PS Pyrolysis and Co-pyrolysis

Based on TG and differential TG (dTG or DTG) analyses, (Table 1 and Fig. 2), three stages can be observed during the pyrolysis of the CNS. The first stage was from room temperature to around 200 °C. This first step may have contributed to the release of the moisture that the shells contained because of the hygroscopic nature of biomass and very light volatiles. The peak temperatures at which this moisture evolution is obtained are between 90 and 112 °C with respect to heating rate. The following mass loss stage was from 190 to 430 °C corresponding to the major mass loss due to the main pyrolytic decomposition. In this stage, much of the weight loss occurred due to the thermal breaking of the bonds in the polymeric structure of the biomass and the formation of stable bonds through secondary reactions. Lignocellulosic biomass is mainly composed of natural biopolymers as hemicelluloses, cellulose, and lignin. It is well known that the main pyrolytic degradation of the lignocellulosic structure is related to the decomposition of hemicellulose (220-315 °C); cellulose (315-400 °C) and lignin degradation (150-450 °C) [41]. The pyrolytic degradation scheme of CNS also reflects the main characteristics of the overlapping zones of the main components. At the last stage of the decom-

Table 1. Pyrolysis characteristics of the samples obtained from TG and dTG curves

Sample	Heating rate (°C/min)	T_i^{*} (°C)	dTG_{max}^{**}	T_f^{***} (°C)	R_p (%/min·mg)	CY (%)
CNS	5	191.03	326.85	380.21	0.19	62.32
	10	197.43	335.49	389.72	0.35	62.25
	20	203.40	342.21	412.46	0.64	60.99
	40	208.71	353.28	431.99	1.60	56.49
PS	5	368.33	422.49	492.54	1.53	4.92
	10	371.93	436.46	506.17	3.46	3.97
	20	373.07	448.65	524.40	6.37	3.39
	40	375.65	466.47	546.42	12.73	3.18
CNS+PS	5	216.90	425.37	499.56	0.73	32.53
	10	222.49	439.47	512.05	1.57	32.30
	20	232.96	452.17	516.25	3.32	32.08
	40	239.86	466.71	542.33	4.60	31.74

*T_i is the initial temperature of the pyrolysis zone

**dTG_{max} is the maximum temperature from the dTG curves

***T_f is the final temperature of the pyrolysis zone

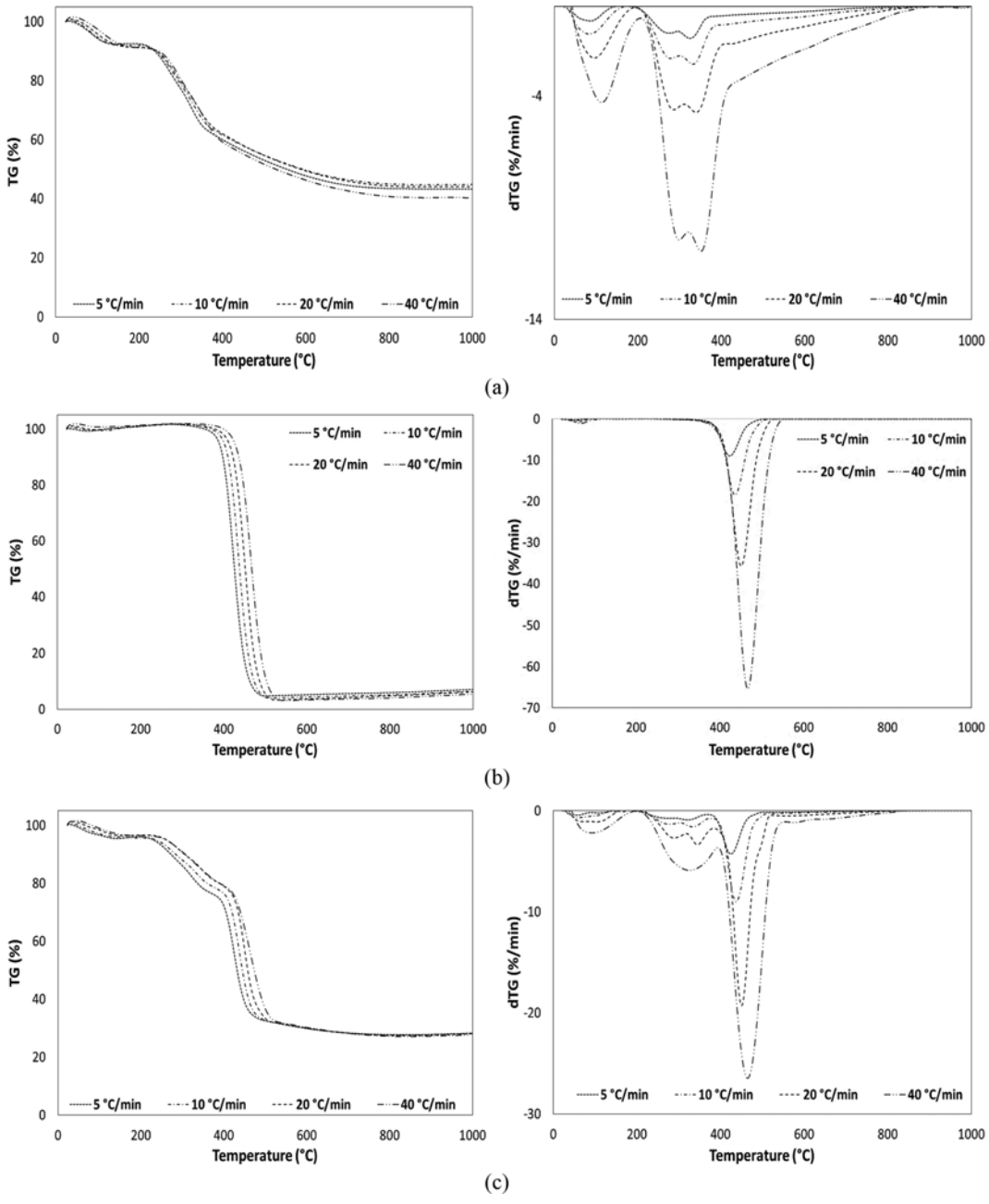

Fig. 2. TG and dTG curves of (a) CNS, (b) PS and (c) CNS+PS.

position, weight loss rate decelerates substantially and TG curves of CNS reach an asymptotic value during this slight decomposition.

On the other hand, TG and dTG curves of PS showed that the mass loss during pyrolysis of PS starts at a higher temperature than CNS, whereas the degradation range of PS is found to be in a narrower temperature range. The maximum mass loss rate of PS is observed at approximately 440 °C. Note that the pyrolytic degradation of PS occurs almost totally in a one-step process that can be well understood from the presence of a single peak in each dTG curve.

The peak temperatures of co-pyrolysis were obtained higher than those of CNS with a higher decomposition intensity. Reactivity indices were found to be increased substantially by adding PS to the biomass. Assuming no interaction between PS and CNS, the pyrolysis characteristics of the blends should follow the behavior of individual feedstock in the mixture. In this respect, theoretical and experimental TG results were calculated at different heating rates, analyzed to understand interactions between PS and CNS and given in Fig. 3. Accordingly, the experimental weight loss values are found greater than those of calculated after 429, 454, 460 and 462 °C, for 5, 10, 20 and 40 °C/min heating rates, respectively. Devolatilization of the components during co-pyrolysis was found to be accelerated and the differences between theoretical and experimental results became obvious in the case of lower heating rates (5 °C/min and 10 °C/min) at the very early stages. On the other

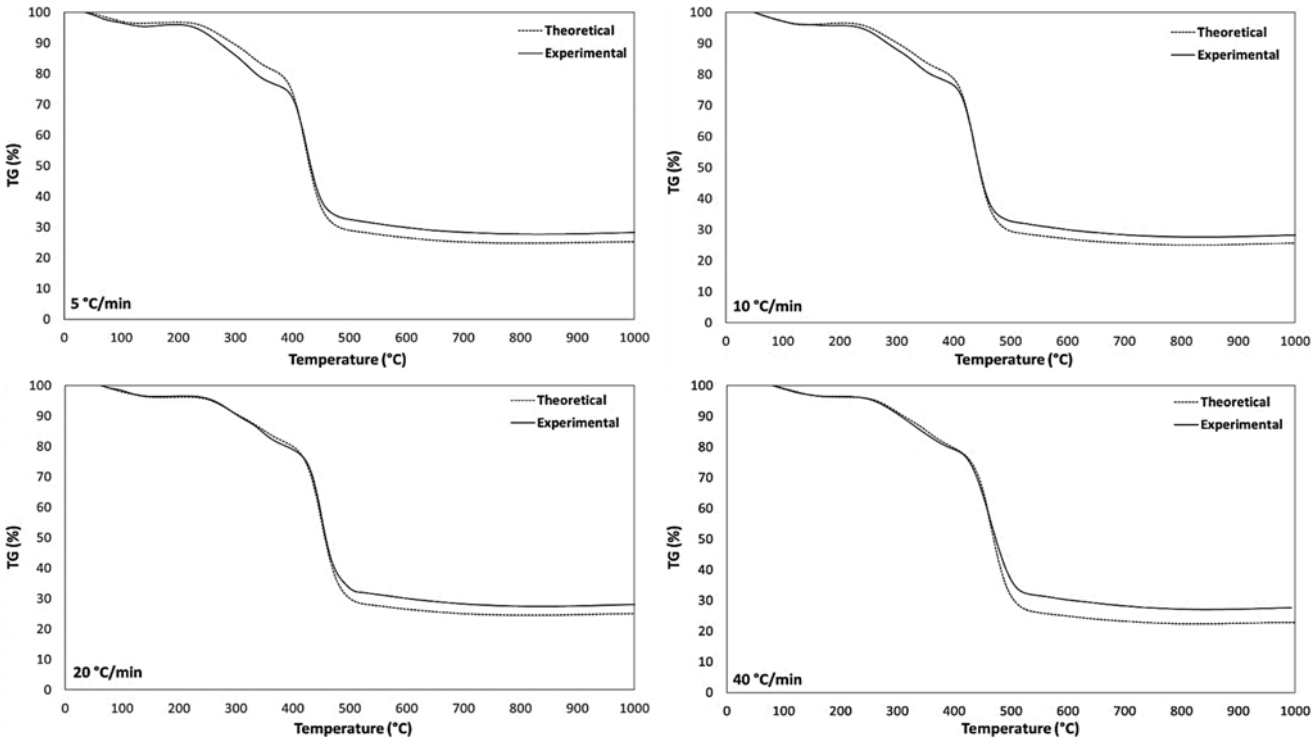

Fig. 3. Theoretical and calculated mass loss curves for co-pyolysis of CNS with PS.

hand, results indicated possible synergistic effect occurring between PS and CNS at elevated temperatures. The differences between experimental and theoretical results may be a consequence of hindering the degradation of each individual material by blending. Possible synergetic effect between CNS and PS may be explained by the radical interactions and hydrogen donors which resulted in differences in theoretical and experimental curves. Because CNS and PS have different H/C ratios and hence hydrogen donor/acceptor mechanism may effect co-pyrolysis mechanism. There is a general consensus about the co-pyrolytic thermal degradation of a different class of raw materials is effected by formation of secondary radicals by reactions such as depolymerization, intermolecular hydrogen transfer and isomerization [42,43].

During the pyrolysis and co-pyrolysis of biomass and PS, increasing heating rates transferred the maximum peak temperatures to the higher values without altering thermal profiles. Thus, the maximum rate of decomposition increased with increasing heating rates because of increasing thermal energy by affecting the temperature difference as well as the temperature gradient. Hence, thermal hysteresis phenomenon is aggravated by increasing the heating rate from 5 to 40 °C/min.

2. Kinetic Analysis Results

We used different heating rates ranging from 5 to 40 °C/min and nine levels of conversion degree varying from 0.10 to 0.90 to determine the dependence of apparent activation energy on the conversion degree. The calculated values are given in Table 2. The corresponding average values of R^2 are all more than 0.98, reflecting that the kinetic analysis of CNS and PS pyrolysis together with

Table 2. Activation energy with respect to conversion degree calculated with DAEM

	CNS		PS		CNS+PS	
α	E_a (kJ/mol)	R^2	E_a (kJ/mol)	R^2	E_a (kJ/mol)	R^2
0.1	153.3	0.9687	220.2	0.9987	141.1	0.9898
0.2	154.5	0.9720	205.3	0.9996	162.0	0.9691
0.3	191.9	0.9746	203.1	0.9995	169.6	0.9473
0.4	196.8	0.9964	207.3	0.9993	211.9	0.9643
0.5	191.8	0.9857	205.0	0.9976	216.2	0.9857
0.6	185.4	0.9957	205.9	0.9986	218.6	0.9992
0.7	175.2	0.9880	209.4	0.9971	206.7	0.9989
0.8	175.3	0.9917	210.8	0.9970	199.2	0.9904
0.9	152.7	0.9933	213.4	0.9973	198.6	0.9919
Average	175.2	0.9851	208.9	0.9983	191.6	0.9818

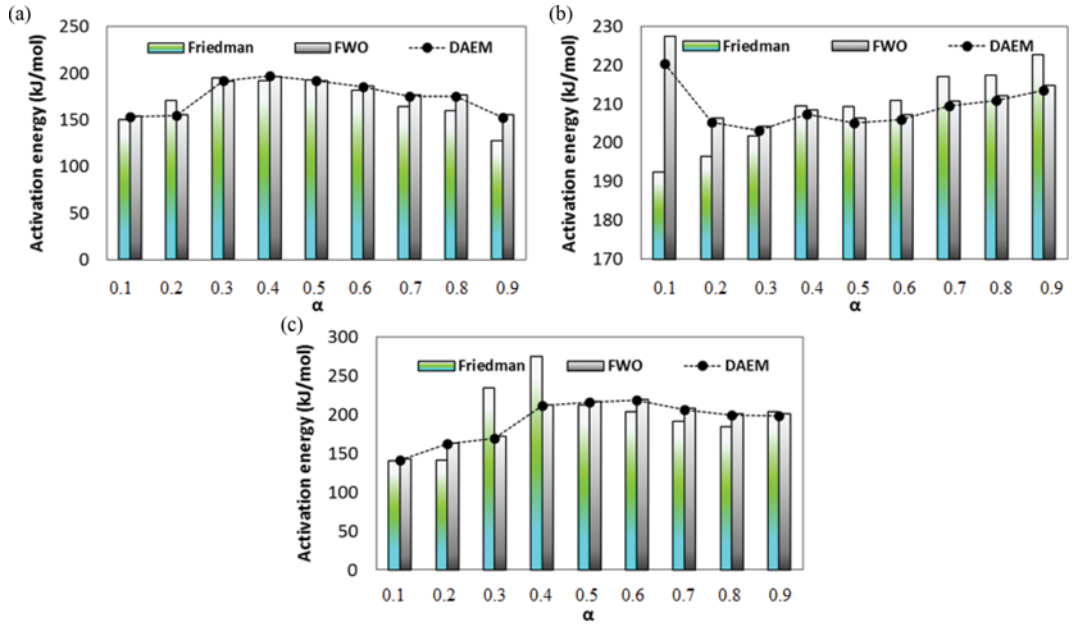

Fig. 4. Activation energy distribitions with respect to conversion degree for (a) CNS, (b) PS and (c) CNS+PS.

co-pyrolysis were well correlated with the DAEM approach.

For CNS pyrolysis, the highest activation energy is observed at a conversion degree of 0.4 as 196 kJ/mol at a temperature around 300 °C. Note that the activation energy values are not constant during degradation of the structure, since they are variable with the progress in conversion degree. The calculated percent deviation values from the average activation energy are found to be between 12.3% and 12.8%. This indicates that there is more than a single reaction mechanism for the pyrolysis of CNS.

On the other hand, during PS pyrolysis, fluctuation of the values of activation energies is not remarkable at between 203 and 220 kJ/mol, and the calculated percent deviation from the average value is between 2.7% to 5.4%. The obtained activation energy values for PS also agree with previous literature studies. Accordingly, the mean activation energy required to degrade the structure of PS is between 188 and 221 kJ/mol [44-49]. Inevitably, differences of PS results are due both to the applied analysis method and structural features of PS, such as molecular weight, end groups, included additives and particle size.

Comparing the calculated mean activation energy of co-pyrolysis with those of the CNS and PS pyrolysis, the energy needed for pyrolysis of PS is clearly decreased by the addition of biomass. Results also show that trends in activation energy with respect to the degree of conversion were also changed substantially by the addition of CNS. It is difficult to describe all of the mechanisms involved in the co-pyrolysis due to the interactions, but it can be concluded that co-pyrolytic behavior of CNS and PS is a complex process involving different reactions. As a result of this phenomenon, the activation energy values of co-pyrolysis are found to be highly dependent on conversion degree. Furthermore, addition to PS to biomass sample seems to decrease the activation energy at the initial stage of co-pyrolysis.

The activation energy values calculated by DAEM were also compared with two different iso-conversional methods, Friedman and FWO. Results were given in Fig. 4. Accordingly, the general trend with respect to conversion degree was found to be similar for CNS, PS pyrolysis, and co-pyrolysis when Friedman and FWO methods applied. Observed quantitative deviations are a result of the assumptions of each kinetic model. For instance, the Friedman method is a differential iso-conversional method that assumes $f(\alpha)$ remains constant and thermal decomposition is independent of temperature and depends only on the rate of mass loss. On the other hand, FWO uses Doyle's approximation to solve p(u) and assumes apparent activation energy remains constant during thermal decomposition in the derivation of the linear model equations.

3. Thermodynamic Analysis Results

To evaluate pyrolytic and co-pyrolytic behaviors of CNS and PS from the viewpoint of thermodynamics, calculated activation energy values using the DAEM approach were used in the calculation of thermodynamic parameters at the maximum conversion rate and are given in Table 3. Since enthalpy change reflects the energy differences between the activated complex and the reagents, it can be an indicator to interpret the nature of pyrolysis and co-pyrolysis processes. If the enthalpy change is small, the potential energy barrier is low and the formation of an activated complex is favored. The smallest enthalpy change value is calculated for biomass pyrolysis at around 170 kJ/mol through the whole pyrolysis range. Addition of PS resulted in an increase of this value, and the highest enthalpy change was observed for PS pyrolysis. So, the formation of an activated complex during biomass pyrolysis seems easier than degradation of polystyrene chains. Besides, positive enthalpy values during pyrolysis and co-pyrolysis showed the main degradation reactions to be endothermic. For CNS pyrolysis, enthalpy change values increased to some extent when conversion degree increased to 0.4. After this value, enthalpy changes were found to be decreased. On the other hand, PS pyrolysis did not show a reg-

Table 3. Thermodynamic parameters calculated with a heating rate of 10 °C/min

α	CNS				PS				CNS+PS			
	A (s^{-1})	ΔH (kj/mol)	ΔG (kj/mol)	ΔS (j/mol)	A (s^{-1})	ΔH (kj/mol)	ΔG (kj/mol)	ΔS (j/mol)	A (s^{-1})	ΔH (kj/mol)	ΔG (kj/mol)	ΔS (j/mol)
0.1	7.1×10^{9}	149.0	169.6	−34.1	8.6×10^{12}	214.6	221.6	−9.9	7.4×10^{6}	135.4	178.5	−58.9
0.2	9.2×10^{9}	150.0	170.4	−33.5	6.4×10^{11}	199.5	213.4	−19.5	2.9×10^{8}	156.9	189.9	−46.3
0.3	1.8×10^{13}	187.3	191.1	−6.2	4.3×10^{11}	197.3	212.1	−20.9	1.1×10^{9}	163.9	194.1	−42.2
0.4	4.9×10^{13}	192.0	193.8	−2.8	9.0×10^{11}	201.4	214.5	−18.4	1.7×10^{12}	206.2	217.5	−15.8
0.5	1.8×10^{13}	186.9	191.0	−6.7	6.1×10^{11}	199.1	213.2	−19.8	3.6×10^{12}	210.4	219.9	−13.3
0.6	4.6×10^{12}	180.5	187.5	−11.5	7.0×10^{11}	199.9	213.7	−19.3	5.5×10^{12}	212.7	221.2	−11.8
0.7	6.1×10^{11}	170.1	181.8	−19.2	1.3×10^{11}	203.4	215.6	−17.2	6.9×10^{11}	200.7	214.5	−19.4
0.8	6.4×10^{11}	170.2	181.9	−19.3	1.7×10^{12}	204.7	216.4	−16.4	1.9×10^{11}	193.2	210.4	−24.2
0.9	6.4×10^{9}	147.4	169.4	−36.1	2.6×10^{12}	207.2	217.8	−14.9	1.7×10^{11}	192.5	210.1	−24.7

ular trend in enthalpy changes with respect to conversion degree due to depolymerization and intermolecular hydrogen transfer. During co-pyrolysis, a similar trend in enthalpy changes was observed as CNS pyrolysis. However, enthalpy change started to decrease after a conversion degree of 0.6 instead of 0.4. When enthalpy change value of co-pyrolysis is compared with the values of the single component at a conversion value of 0.1, it is obviously seen that PS effects degradation of biomass at the initial stage of the process.

Another thermodynamic function, entropy change, shows how near the system is to its own thermodynamic equilibrium. In the case of low activation entropy values, it is accepted that material has just passed through some kind of process, bringing it to a state near its own thermodynamic equilibrium. In this case, reactants show little reactivity; so time to form the activated complex is increased. Otherwise, the material is far from its own thermodynamic equilibrium when high activation entropy values are present. In such a situation, the reactivity is high and the system can react faster to produce the activated complex, which results in short reaction times. Based on negative values of entropy change, disorder degree of the evolved products through pyrolytic and co-pyrolytic degradation is lower than that of raw materials.

When it comes to Gibbs free energy change, it can be illustrated as a comprehensive evaluation of disorder change, since it indicates the total energy increase of the system at the approach of the reagents and the formation of the activated complex. In the case of lower Gibbs free energy change, a higher favorability of reaction is indicated. At the initial stages of PS pyrolysis Gibbs free energy change was found as 221.6 kJ/mol, and then it decreased as degradation proceeded and slightly increased at the last stage of pyrolysis. But the changes and deviations from the average value were obtained smaller compared to CNS and CNS+PS pyrolysis. On the other hand, CNS pyrolysis and co-pyrolysis processes showed a similar Gibbs free energy change distribution like enthalpy distribution throughout the conversion range. It may be a result that biomass addition to PS favors cracking of the structure at the very early stages of pyrolysis.

When the calculated pre-exponential factors were examined, some variations with respect to conversion degree were also obvious. Pre-exponential factors of CNS changed from 6.4×10^{9} to 4.9×10^{13} s^{-1}. On the other hand, PS presented values of pre-exponential factors between 1.3×1011 and 8.6×10^{12} s^{-1}. Different from each component, calculated pre-exponential values of co-pyrolysis of CNS and PS varied from 7.4×10^{6} to 5.5×10^{12} s^{-1}, which indicates the interactions between polymer and lignocellulosic structure. The observed fluctuations clearly illustrate that complex reaction mechanisms and interaction of the radicals occur during pyrolytic decomposition.

4. TG/FT-IR/MS Results

The outputs from online FT-IR analyses are three-dimensional (3-D) plots that indicate IR spectra as a function of time. The obtained 3-D plots are given in Fig. 5. Exact detection of band positions in such analyses is complicated because of the complex mechanisms and overlapping zones occur during online analysis. But it is convenient to say that the most obviously seen intense peak in 3-D spectra of CNS is of asymmetric C=O stretching vibration (2,250-2,500 cm^{-1}) due to the removal of carbonyl functional groups. This peak is a result of cracking and reforming reactions of lignocellulosic biomass. This carbon dioxide evolution during the degradation process can also be confirmed by the C=O bending

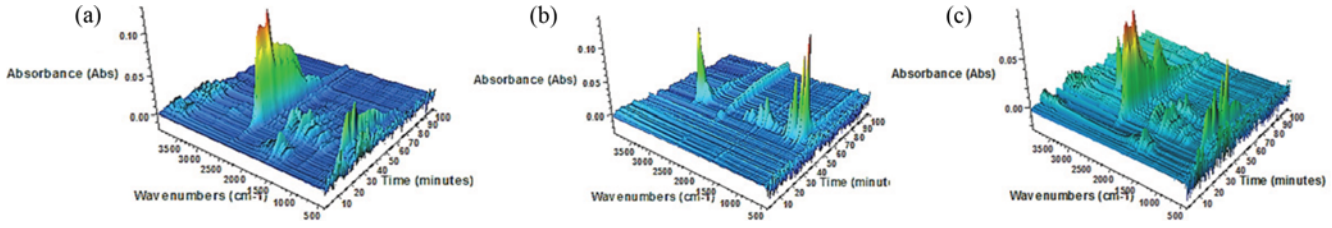

Fig. 5. 3-Dimensional FT-IR spectra of (a) CNS, (b) PS and (c) CNS+PS.

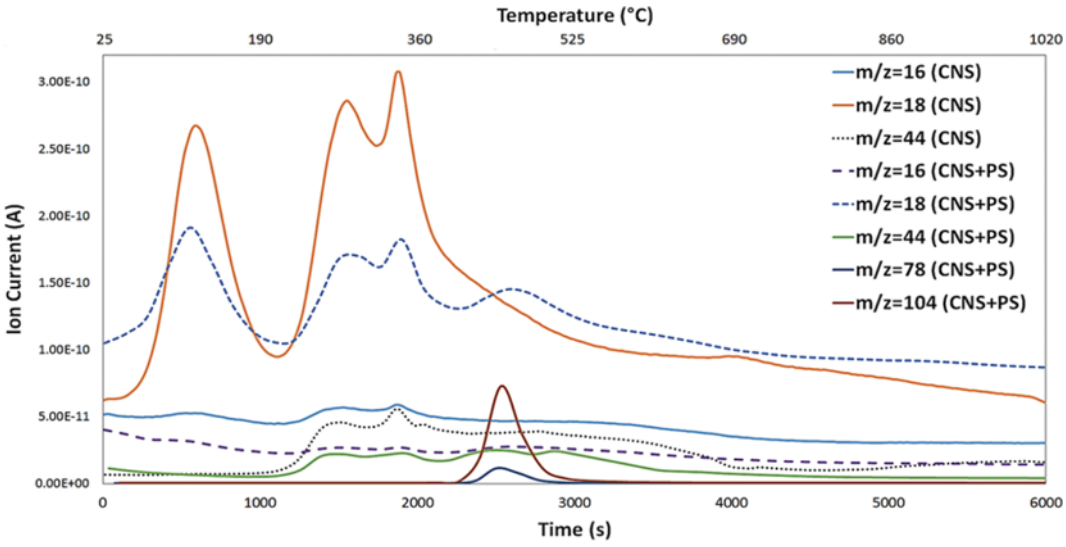

Fig. 6. Single ion current curves for major evolved species during pyrolysis (β=10 °C/min).

vibrations (580-730 cm^{-1}). Carbon dioxide evolution is seen in a broad temperature range between 200 and 900 °C as a result of the main decomposition of the lignocellulosic structure in pyrolysis zone followed by charring of the remaining structure and gasification at higher temperatures. Smaller carbonyl C=O stretching vibrations (1,750-1,650 cm^{-1}) indicate the release of aldehydes, ketones, and carboxylic acids. Besides, O-H stretching vibrations (3,400-3,800 cm^{-1}) are observed both at the initial water removal stage and main pyrolysis zone due to the release of water. This water removal is not only a result of moisture removal but also dehydration reactions. This O-H band (960-1,085 cm^{-1}) also indicates the release of phenolics, acids, and alcohols together with stretching [50].

Compared to the spectra of the CNS, PS pyrolysis seems much simpler, which supports the single reaction scheme. According to spectra, C-H stretching vibrations (3,300-3,000 cm^{-1}) and in-plane bending vibrations (1,300-1,000 cm^{-1}) of mononuclear aromatic hydrocarbons are noticeable. Other skeletal vibrations of mononuclear hydrocarbons (1,500-1,400 cm^{-1}) together with out of plane C-H bending vibrations (910 and 670 cm^{-1}) of mononuclear hydrocarbons also appeared in the spectra. =C-H stretching (3,100-3,000 cm^{-1}) and C=C stretching (1,700-1,600 cm^{-1}) vibrations were also observed in the 3-D spectra of PS. During the degradation C-C bond cleavage and formation of free radicals occurs. These free radicals react with polystyrene to produce short-chain radicals. According to the results, it is suggested that the main reaction during pyrolysis is depolymerization of PS to styrene monomers by yielding small amounts of radicals that may also be understood from the fingerprint region between 1,000 and 500 cm^{-1}.

When the 3-D FT-IR profile of the co-pyrolysis is examined, it can be obviously concluded that the addition of the profiles obtained from CNS and PS pyrolysis has changed slightly. For instance, additional formation steps of CO_2 and aromatic chains were observed due to the radicals. This suggests that some degree of chemical interaction may occur during the co-pyrolysis of CNS and PS. The band between 2,800 and 3,150 cm^{-1} is attributed to -CH_2 and -CH_3 stretching vibrations that are mainly due to the presence of methane gas in the volatiles. Methane is formed as a result of the decomposition of methoxy, methyl and methylene groups.

Online MS analyses were also performed simultaneously with the FT-IR analyses since FT-IR spectra give only qualitative information about the functional group of the evolved pyrolysis products. To observe the effect of PS mixing to biomass, mass spectra were obtained for a wider array of species. But target signals with m/z ratios (m/z) of 16, 18, 44, 78 and 104 (which indicate the evolution of methane, water, carbon dioxide, benzene, and styrene, respectively) were considered for discussion and are given in Fig. 6. Signals belonging to benzene and styrene supported the depolymerization of styrene which showed a maximum peak around 450 °C. On the other hand, methane, water, and carbon dioxide evolution profiles were changed considerably, which indicates changes in reaction mechanisms and synergic effects in the case of co-pyrolysis. For instance, additional water and carbon dioxide evolution steps were observed. Therefore, it is convenient to say that PS addition triggered dehydration and the decarboxylation reactions at the final stage of decomposition (approximately between 370 and 500 °C).

CONCLUSIONS

Pyrolytic and co-pyrolytic degradation behaviors of CNS and PS were reported. Simultaneous TGA/FT-IR/MS analyses of CNS, PS, and their blend were performed at four linear heating rates, simulating a pyrolysis process. The differences in thermal behaviors are explained by the number of mass loss steps, their percentages, and their temperature ranges.

After that, pyrolysis and kinetics were examined using DAEM approach. The TGA data were well described by DAEM and the results were compared with Friedman and FWO methods.

The results of both thermogravimetric and kinetic analyses implied that the co-pyrolysis characteristics of PS and CNS are quite different from the combination of the individual materials. Hence, there

may exist some interactions and synergic effects between PS and CNS co-pyrolysis.

The main evolved gases released during thermal degradation were detected by online FT-IR and MS measurements and supported the interactions among the radicals produced by CNS and PS degradation.

Regarding thermodynamic analysis, complex reaction mechanisms and interaction of the radicals occurring during co-pyrolytic decomposition were expressed in terms of thermodynamic parameters.

REFERENCES

1. K. Ragaert, L. Delva and K. Van Geem, *Mechanical and chemical recycling of solid plastic waste*, *Waste Manage.*, Article in Press (2017).
2. Plastics Europe, EuPC, EPRO (2015) Plastics - The Facts 2015: An Analysis of European Plastics Production, Demand and Recovery for 2015.
3. European Commission Energy Strategy and Energy Union Website, http://ec.europa.eu/energy/en/topics/energy-strategy-and-energy-union/2020-energy-strategy.
4. A. Mukherjee, P. Das and K. Minu, *Biomass Conversion and Biorefinery*, **4**(3), 259 (2014).
5. I. Bekri-Abbes, S. Bayoudh and M. Baklouti, *J. Polym. Environ.*, **14**(3), 249 (2006).
6. R. Sinha, S. Kumar and R. Singh, *Biomass Conversion and Biorefinery*, **3**(4), 327 (2013).
7. M. R. Othman, Y.-H. Park, T. A. Ngo, S.-S. Kim, J. Kim and K. S. Lee, *Korean J. Chem. Eng.*, **27**(1), 163 (2010).
8. E. Butler, G. Devlin and K. McDonnell, *Waste and Biomass Valorization*, **2**(3), 227 (2011).
9. T. R. Kosanić, M. B. Ćeranić, S. N. Đurić, V. R. Grković, M. M. Milotić and S. D. Brankov, *J. Therm. Sci.*, **23**(3), 290 (2014).
10. S. Polesek-Karczewska and D. Kardaś, *J. Therm. Sci.*, **24**(1), 82 (2015).
11. R. Soysa, Y. S. Choi, S. K. Choi, S. J. Kim and S. Y. Han, *Korean J. Chem. Eng.*, **33**(2), 603 (2016).
12. A. Pollex, A. Ortwein and M. Kaltschmitt, *Biomass Conversion and Biorefinery*, **2**(1), 21 (2012).
13. A. Nzihou, B. Stanmore and P. Sharrock, *Energy*, **58**, 305 (2013).
14. S. Junpirom, C. Tangsathitkulchai and M. Tangsathitkulchai, *Korean J. Chem. Eng.*, **27**(3), 791 (2010).
15. B. S. Santos and S. C. Capareda, *Biomass Conversion and Biorefinery*, **6**(3), 325 (2016).
16. I. Y. Mohammed, C. H. Lim, F. K. Kazi, S. Yusup, H. L. Lam and Y. A. Abakr, *Waste and Biomass Valorization*, **8**(3), 911 (2016).
17. L. Chen, S. Wang, H. Meng, Z. Wu and J. Zhao, *Appl. Therm. Eng.*, **111**, 834 (2017).
18. M. Brebu, S. Ucar, C. Vasile and J. Yanik, *Fuel*, **89**(8), 1911 (2010).
19. S. Al-Salem and P. Lettieri, *Chem. Eng. Res. Design*, **88**(12), 1599 (2010).
20. H. W. Lee, S. J. Choi, S. H. Park, J.-K. Jeon, S.-C. Jung, S. C. Kim and Y.-K. Park, *Nanoscale Res. Lett.*, **9**(1), 376 (2014).
21. S. A. Sakaki, B. Roozbehani, M. Shishesaz and N. Abdollahkhani, *Clean Technologies and Environ. Policy*, **16**(5), 901 (2014).
22. J. Shah, *J. Polym. Environ.*, 1 (2014).
23. I. Barbarias, G. Lopez, J. Alvarez, M. Artetxe, A. Arregi, J. Bilbao and M. Olazar, *Chem. Eng. J.*, **296**, 191 (2016).
24. B. Han, Y. Chen, Y. Wu, D. Hua, Z. Chen, W. Feng, M. Yang and Q. Xie, *J. Therm. Anal. Calorimetry*, **115**(1), 227 (2014).
25. J. Chattopadhyay, T. Pathak, R. Srivastava and A. Singh, *Energy*, **103**, 513 (2016).
26. S. Xiong, J. Zhuo, H. Zhou, R. Pang and Q. Yao, *J. Analytical Appl. Pyrol.*, **112**, 66 (2015).
27. Y.-M. Kim, T. U. Han, B. Hwang, B. Lee, H. W. Lee, Y.-K. Park and S. Kim, *Korean J. Chem. Eng.*, **33**(8), 2350 (2016).
28. J. Alvarez, S. Kumagai, C. Wu, T. Yoshioka, J. Bilbao, M. Olazar and P. T. Williams, *Int. J. Hydrogen Energy*, **39**(21), 10883 (2014).
29. A. K. Varma and P. Mondal, *J. Therm. Anal. Calorimetry*, **124**(1), 487 (2016).
30. S. A. El-Sayed and M. E. Mostafa, *Waste and Biomass Valorization*, **6**(3), 401 (2015).
31. J. Wang and H. Zhao, *Waste and Biomass Valorization*, **6**(4), 527 (2015).
32. R. R. Pradhan, P. P. Garnaik, B. Regmi, B. Dash and A. Dutta, *Biomass Conversion and Biorefinery*, **7**, 237 (2017).
33. A. Malika, N. Jacques, B. Fatima and A. Mohammed, *Biomass Conversion and Biorefinery*, **6**(2), 161 (2016).
34. Y. Ma, J. Wang and Y. Zhang, *Biomass Conversion and Biorefinery*, 1 (2017).
35. Food and Agriculture Organization of the United Nations Website http://www.fao.org/home/en/.
36. J. E. White, W. J. Catallo and B. L. Legendre, *J. Analytical Appl. Pyrol.*, **91**(1), 1 (2011).
37. K. Miura and T. Maki, *Energy Fuels*, **12**(5), 864 (1998).
38. H. L. Friedman, Kinetics of thermal degradation of char-forming plastics from thermogravimetry. Application to a phenolic plastic. In: Journal of Polymer Science: Polymer Symposia, 1964. vol 1. Wiley Online Library, pp. 183-195.
39. T. Ozawa, *Bulletin Chem. Soc. Japan*, **38**(11), 1881 (1965).
40. J. H. Flynn and L. A. Wall, *J. Res. Nat. Bur. Stand.*, **70**(6), 487 (1966).
41. H. Yang, R. Yan, H. Chen, D. H. Lee and C. Zheng, *Fuel*, **86**(12), 1781 (2007).
42. Ö. Çepelioğullar and A. E. Pütün, *J. Analytical Appl. Pyrol.*, **110**, 363 (2014).
43. F. Abnisa and W. M. A. W. Daud, *Energy Convers. Manage.*, **87**, 71 (2014).
44. R. Westerhout, J. Waanders, J. Kuipers and W. Van Swaaij, *Ind. Eng. Chem. Res.*, **36**(6), 1955 (1997).
45. K. Murata, Y. Hirano, Y. Sakata and M. A. Uddin, *J. Analytical Appl. Pyrol.*, **65**(1), 71 (2002).
46. R. Aguado, B. Gaisán, R. Prieto and J. Bilbao, *Chem. Eng. J.*, **92**(1), 91 (2003).
47. W.-R. Zeng, Y.-J. Zhou, R. Huo, B. Yao and Y.-Z. Li, *Gaofenzi Cailiao Kexue yu Gongcheng/Polymer Materials Science Engineering*, **22**(5), 162 (2006).
48. A. Meng, S. Chen, Y. Long, H. Zhou, Y. Zhang and Q. Li, *Waste Manage.*, **46**, 247 (2015).
49. J. Cheng, Y. Pan, J. Yao, X. Wang, F. Pan and J. Jiang, *Journal of Loss Prevention in the Process Industries*, **40**, 139 (2016).
50. G. Özsin and A. E. Pütün, *Waste Manage.*, **64**, 315 (2017).